EUROPEAN JOURNAL OF PURE AND APPLIED MATHEMATICS
2026, Vol. 19, Issue 2, Article Number 6591
ISSN 1307-5543 – ejpam.com
Published by New York Business Global

Fuzzy Fractal–Fractional Differential Framework for Pneumonia Transmission Dynamics

M. Tamil Vizhi[1], J. Vimala[1,*], P. Mahalakshmi[1], Dragan Pamucar[2,*]

[1] *Department of Mathematics, Alagappa University, Karaikudi, Tamilnadu, India*
[2] *Széchenyi István University, Győr, Hungary*

Abstract. Pneumonia caused by *Streptococcus pneumoniae* remains a major public health concern, especially in vulnerable populations. Its transmission is affected by uncertain and irregular factors such as environmental changes, contact variability, and imprecise clinical data. This study introduces a novel fuzzy fractal–fractional mathematical model incorporating epidemiological compartments: susceptible, exposed, infected, vaccinated, and recovered groups. To handle uncertainties in biological parameters, fuzzy logic is applied, while the fractal–fractional Atangana–Baleanu operator captures memory and hereditary effects in disease transmission. Theoretical analysis confirms the existence, uniqueness, and Ulam–Hyers stability of the model. Numerical solutions are derived using Lagrange polynomial interpolation. Simulation results show a decline in exposed and infected populations within 20–30 time units, while vaccinated and recovered classes steadily increase and stabilize. The susceptible population also reaches a steady state, indicating potential disease control under uncertain conditions. Compared to classical and standard fractional models, the proposed model achieves improved convergence and better accommodates parameter imprecision. Overall, this integrated fuzzy fractal–fractional approach enhances the accuracy and robustness of pneumonia modeling, offering a valuable framework for analyzing infectious diseases under uncertainty in public health settings.

2020 Mathematics Subject Classifications: 34A07, 34K36

Key Words and Phrases: Fractal-fractional operator, mittag-Leffler kernel, fuzzy number, gH-difference

1. Introduction

Pneumonia is a serious respiratory infection that affects the lungs and causes inflammation of the air sacs. These air sacs are filled with fluid or pus, leading to shortness of breath. Other common symptoms include coughing, fever, and chills. The disease is caused by various pathogens, such as bacteria, viruses, and fungi. Pneumonia can range

*Corresponding Authors.
DOI: https://doi.org/10.29020/nybg.ejpam.v19i2.6591

Email addresses: tamilvizhi2502@gmail.com (M. Tamil Vizhi),
vimaljey@alagappauniversity.ac.in (J. Vimala)
mahalakshmi4812@gmail.com (P. Mahalakshmi), dpamucar@gmail.com (Dragan Pamucar)

 Copyright: © 2026 The Author(s). (CC BY-NC 4.0)

from mild to severe and is associated with the elderly, young children, and people with weakened immune systems[1, 2]. The diagnosis typically involves a combination of physical examination, chest radiographs, and laboratory tests. Treatment includes antibiotics for bacterial pneumonia, along with rest, hydration, and oxygen therapy in severe cases. Prevention measures include vaccination, good hygiene practices, and avoiding smoking [3, 4]. Among the pathogens, *Streptococcus pneumoniae* is a major bacterial cause and has more than 90 serotypes. This bacterium often lives in the respiratory tract and is carried by children and healthcare workers[5, 6].

In many developing countries, pneumonia remains one of the leading causes of death in children, often linked to the prevalence of HIV and poor access to healthcare[7, 8]. Research shows that children with S. pneumoniae are more likely to require hospitalization[9, 10]. In Africa, non-vaccinated children show carriage rates ranging from 7% to 90% [11–13]. Despite available treatments, the increase in antibiotic-resistant strains has increased the risk of infection. As a result, early interventions such as vaccination and short-course antibiotic treatment are critical[14].

Mathematical models have played an essential role in analyzing their transmission and supporting intervention strategies. Early models using classical differential equations provided insight into stability and control measures, while later studies incorporated treatment, vaccination, and optimal control approaches to improve predictions[15–17]. Serotype-specific models and household transmission analyzes refined our understanding of infection patterns. Recent research [18] has dealt with the fractional-order SVEIR framework and incorporated memory effects and partial immunity. This has shown that increased vaccination and recovery rates can lead to disease elimination when the reproduction number falls below one. Although these models often overlook uncertainty in key parameters.

Traditional differential equations are essential for modeling dynamic processes, but they often struggle to capture memory effects and irregular behaviors. Fractional differential equations extend classical calculus through the non-integer derivatives and improve the accuracy of models from disease dynamics to industrial applications. The limitations of fractional differential equations are faced when dealing with fractal-like structured systems, and this led to the introduction of fractal-fractional differential equations.

Atangana [19] introduced the fractal–fractional differential equations by integrating the fractional calculus with fractal geometry, and these models consider both a fractional order and fractal dimension and achieve better representations of non-smooth dynamics[20]. Recent studies have demonstrated the effectiveness of fractal–fractional operators in modeling viral diseases such as monkeypox and viral diarrhea[21, 22], showing an improved data fit compared to classical and purely fractional models[23–25].

Based on Zadeh's fuzzy set theory, fuzzy derivatives have been formulated to deal with uncertainty in parameters and initial conditions[26]. Using fuzzy numbers and generalized Hukuhara (gH) derivatives[27], these models accommodate ambiguous or imprecise data without oversimplification[6]. Researchers have recognized the need for a comprehensive approach and proposed fuzzy fractal–fractional differential equations to integrate memory effects and uncertainty handling[28, 29]. This unified framework offers the most

essential tool for modeling complex biological and epidemiological systems, including infectious diseases such as pneumonia under uncertain conditions[30, 31]. Motivated by recent applications of fuzzy logic in healthcare diagnostics, COVID-19 decision support, and environmental monitoring [32–34], we aim to extend these ideas to pneumonia modeling under uncertainty. The recent developments in fuzzy-based multi-criteria decision systems, renewable energy selection, and cybersecurity frameworks [35–37] support the broader applicability of such hybrid intelligent models in complex systems.

1.1. Literature Review

Understanding the spread and control of pneumonia has long been a focus of infectious disease modeling. Over the years, researchers have developed mathematical models from classical ordinary differential equation frameworks to fractional differential approaches.

One of the earlier models [18] was developed to analyze the transmission of pneumonia among children under five years of age, a group at high risk of infection and mortality. The model was formulated using ordinary differential equations and investigated equilibrium points and performed a bifurcation analysis. Building on this foundation, [38] introduced a model designed to assess the impact of treatment and vaccination strategies on pneumococcal pneumonia among children. Treatment alone was shown to be insufficient, highlighting the importance of a comprehensive approach to pneumonia control. In [39], a model was developed to evaluate childhood pneumonia in Kenya, and focusing on local epidemiological conditions. The study emphasized that interventions for improved vaccination, increased treatment rates, and environmental management were crucial in reducing the burden of the disease. The researchers [40] proposed a model that incorporates serotype-dependent transmission of Streptococcus pneumoniae. This model revealed that the strain with the higher reproduction number tends to dominate and has implications for vaccine development and deployment. The study [16] examined the genetic variation and serotype switching, showing how a single sequence type could manifest as either a vaccine or non-vaccine serotype and how this affects disease persistence. More recent works have explored control strategies and cost-effectiveness. In [41], a model examined treatment and screening interventions and concluding that the combination of both was more effective than either alone. Similarly, [42] applied optimal control theory to assess education, treatment, and screening strategies. The findings supported the idea that prevention combined with treatment is the most cost-effective approach for managing pneumonia spread.

Real-world data-driven insights were provided in [17], which analyzed *S. pneumoniae* transmission in households in the UK. Using swab data from 121 families, the study fitted a density-dependent model and found that children under five had longer carriage durations and were more likely to acquire the infection. Adults were more infectious but less susceptible. In-household transmission highlights the need for targeted public health interventions. Another recent contribution [43] uses an SVEIR model to assess the role of vaccination in pneumonia control.

A key advancement in pneumonia modeling is the introduction of fractional calculus.

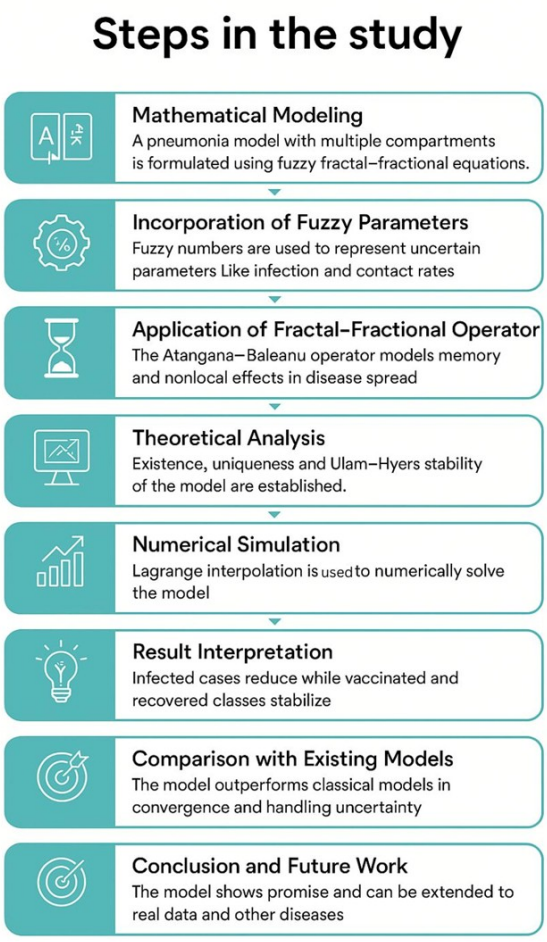

Figure 1: Workflow of the study

The foundational work[44] presents a fractional SVEIR model that investigates the spread of pneumonia, and the model accounts for partial immunity, indicating that individuals with high antibody levels do not require revaccination. It highlights the importance of increasing recovery rates, which contributes to a decrease in infection levels over time. Although this model offers powerful insights, it notes some limitations: it may not accurately capture the dynamics among vulnerable populations, and its predictions heavily depend on precise estimation of key parameters such as transmission and infectiousness rates. The model presented stands out for its use of fractional calculus and partial immunity mechanisms to understand the dynamics of pneumonia. Further improvements, such as integrating fuzzy parameters to address real-world uncertainty, remain necessary. These observations motivate the current work and propose a fractal–fractional model with fuzzy parameters to more accurately reflect the transmission of pneumonia under uncertainty.

Motivation

Pneumonia remains a significant global health burden, especially among vulnerable populations where timely detection and intervention are critical. Traditional mathematical models often fail to capture the uncertainty and memory-dependent nature of disease dynamics. Motivated by this limitation, the present study integrates fuzzy logic and fractal–fractional calculus to provide a more realistic and robust description of pneumonia transmission.

Contribution of the Study

This study proposes a novel fuzzy fractal–fractional model for pneumonia dynamics, incorporating biological imprecision through fuzzy logic and memory effects via the Atangana–Baleanu fractal–fractional operator. The existence, uniqueness, and Ulam–Hyers stability of the model are mathematically established. A Lagrange polynomial interpolation scheme is used for the numerical simulation of the system, enabling the evaluation of disease behavior under uncertain conditions.

Research Gaps

Conventional and classical fractional models inadequately handle both memory effects and uncertainty in parameters simultaneously. There is a lack of literature integrating fuzzy systems with fractal–fractional operators, particularly in the context of infectious disease modeling. Most existing studies do not provide rigorous theoretical backing such as Ulam–Hyers stability under fuzzy environments. Moreover, numerical comparisons with classical and fractional models are rarely conducted to validate the impact of uncertainty. This study fills these research gaps by presenting a hybrid fuzzy fractal–fractional model, supported by strong analytical and computational results.

Structure of the Manuscript

Section 2 provides the fundamental definitions that set the groundwork for the study.

Section 3 presents the mathematical formulation of the fuzzy fractal–fractional pneumonia model. Each compartment in the population and the parameters are described in detail.

Section 4 is devoted to the existence and uniqueness of solutions to the proposed system. The analysis is established using Schauder's and Banach's fixed-point theorems.

Section 5 investigates the Ulam–Hyers stability of the model to assess how small perturbations in the system influence the long-term behavior of solutions.

Section 6 provides the numerical results and discussion. The model is solved using Lagrange piecewise interpolation and the results are illustrated graphically. The implications of the results and the key findings are reported in 6.1

Section 7 offers a comparative analysis between the proposed fuzzy fractal–fractional model and an existing fractional-order model [44], highlighting improvements in memory

handling, uncertainty treatment, and system behavior.
The sequential methodology adopted in this study is illustrated in Figure 1.

2. Preliminaries

Definition 1. *[45] A fuzzy membership function $\tilde{\mathfrak{u}} : \mathbb{R} \to [0,1]$ is a fuzzy number if $\tilde{\mathfrak{u}}$ is convex, normal, upper semi-continuous and the closure of its support is compact.*

Definition 2. *[45] A fuzzy number $\tilde{\mathfrak{u}}$ is defined in the parametric form $[\tilde{\mathfrak{u}}]_\alpha = [\underline{\dot{u}}(\alpha), \overline{\dot{\mathfrak{u}}}(\alpha)]$, where $0 \leq \alpha \leq 1$ and*

(i) *$\underline{\dot{u}}(\alpha)$ is increasing left continuous on $\alpha \in (0,1]$ and right continuous at 0.*

(ii) *$\overline{\dot{\mathfrak{u}}}(\alpha)$ is decreasing left continuous on $\alpha \in (0,1]$ and right continuous at 0.*

(iii) *$\underline{\dot{u}}(\alpha) \leq \overline{\dot{\mathfrak{u}}}(\alpha)$, $\forall\ \alpha \in [0,1]$.*

Definition 3. *[19] The fractal-fractional derivative with fractional order γ of a fractal differentiable $\mathcal{A}(t)$ function, in Riemann-Liouville sense is given as:*

$$\mathbb{D}_{\gamma,\rho}(\mathcal{A}(t)) = \frac{M_{\mathrm{AB}}(\gamma)}{1-\gamma}\frac{d}{dt^\rho}\int_0^t \Xi_\gamma\left[-\frac{\gamma}{1-\gamma}(t-s)^\gamma\right]\mathcal{A}(s)ds, \tag{1}$$

where normalizer function is $M_{\mathrm{AB}}(\gamma)$ = 1 - γ + $\frac{\gamma}{\Gamma(\gamma)}$ and Mittag-Leffler Kernel is $\Xi_\gamma(t)$ = $\sum_{n=0}^{\infty} \frac{t^n}{\alpha t+1}$.

Definition 4. *[19] The fractal-fractional integral with fractional order of γ is formulated as:*

$$\mathbb{I}_{\gamma,\rho}(\mathcal{A}(t)) = \frac{(1-\gamma)\rho t^{\rho-1}}{M_{\mathrm{AB}}(\gamma)}\mathcal{A}(t) + \frac{\gamma\rho}{M_{\mathrm{AB}}(\gamma)\Gamma(\gamma)}\int_0^t s^{\rho-1}(t-s)^{\gamma-1}\mathcal{A}(s)ds \tag{2}$$

Definition 5. *[45] Arithmetic operations on fuzzy numbers $\tilde{\mathfrak{u}}_1$, $\tilde{\mathfrak{u}}_2$ and $\tilde{\mathfrak{u}}_3$ are*

- $[\tilde{\mathfrak{u}}_1 \oplus \tilde{\mathfrak{u}}_2]_\alpha = [\underline{\dot{u}}_1(\alpha) + \underline{\dot{u}}_2(\alpha),\ \overline{\dot{\mathfrak{u}}}_1(\alpha) + \overline{\dot{\mathfrak{u}}}_2(\alpha)]$,
- *For* $\eta \in \mathbb{R}$, $[\eta \odot \tilde{\mathfrak{u}}]_\alpha = \begin{cases} [\eta\underline{\dot{u}}(\alpha), \eta\overline{\dot{\mathfrak{u}}}(\alpha)], & \text{if } \eta \geq 0 \\ [\eta\overline{\dot{\mathfrak{u}}}(\alpha), \eta\underline{\dot{u}}(\alpha)], & \text{if } \eta < 0, \end{cases}$
- $[\tilde{\mathfrak{u}}_1 \ominus \tilde{\mathfrak{u}}_2]_\alpha = [\min\{\underline{\dot{u}}_1(\alpha) - \underline{\dot{u}}_2(\alpha),\ \overline{\dot{\mathfrak{u}}}_1(\alpha) - \overline{\dot{\mathfrak{u}}}_2(\alpha)\}, \max\{\underline{\dot{u}}_1(\alpha) - \underline{\dot{u}}_2(\alpha),\ \overline{\dot{\mathfrak{u}}}_1(\alpha) - \overline{\dot{\mathfrak{u}}}_2(\alpha)\}]$

where $\ominus$ is Generalized Hukuhara difference operation.

Table 1: Outline of the parameters

Parameter	**Description**	**Value**
$\mathfrak{a}$	The vaccination coverage rate	0.2 [38]
1-$\mathfrak{a}$	The susceptibility rate within a subset of herds	0.8
$\mathfrak{b}$	Susceptible class entry rate	10.09 [38]
$\mathfrak{c}$	The amount of susceptibility within the vaccinated class	0.0621 [38]
$\mathfrak{d}$	Recovery to susceptible transition rate	5.4 [Assumed]
$\mathfrak{e}$	The vaccination degree within the susceptible class	0.15 [44]
$\mathfrak{f}$	The rate of natural mortality	0.2 [38]
$\mathfrak{h}$	Effectiveness of vaccination	0.3 [43]
$\mathfrak{j}$	The degree of recovery through natural immune protection	0.00083 [44]
$\tilde{\mathfrak{k}}$	The degree of infection within the exposed class	[0.01+0.00096α, 0.01192-0.00096α]
$\ddot{\mathcal{E}}$	Infection-induced mortality rate	0.0002 [Assumed]
$\mathfrak{m}$	The rate of recovery within the infection class	0.0714 [38]
$\mathfrak{n}$	The temporary immunity waning rate within the recovered class	0.007 [44]
$\tilde{\delta}$	Effective contact rate	[0.01+0.0187α, 0.0474-0.0187α]
σ	Antibiotics production rate of infected individual	8 [44]

Definition 6. *[45] The Hausdorff distance* $\varrho : F_{\mathbb{R}} \times F_{\mathbb{R}} \to \mathbb{R}^+ \cup \{0\}$ *is formulated by*

$$\varrho(\tilde{\mathfrak{u}}, \tilde{\mathfrak{v}}) = \sup_{\alpha\in[0,1]} \max\{|\underline{u}(\alpha) - \underline{v}(\alpha)|, |\overline{\mathfrak{u}}(\alpha) - \overline{\mathfrak{v}}(\alpha)|\},$$

where $F_{\mathbb{R}}$ *is the space of all fuzzy numbers.*

3. Pneumonia Model

The model pneumonia [44] integrated the recovery, immunization, and vaccination processes for better understanding of the dynamics of pneumonia. The model is derived as:

$$\begin{aligned}
\frac{d\ddot{\mathcal{S}}}{dt} &= (1-\mathfrak{a})\mathfrak{b} + \mathfrak{c}\ddot{\mathcal{V}}(t) + \mathfrak{d}\ddot{\mathcal{R}}(t) - (\mathfrak{e}+\mathfrak{f}+\mathfrak{g})\ddot{\mathcal{S}}(t)\\
\frac{d\ddot{\mathcal{V}}}{dt} &= \mathfrak{a}\mathfrak{b} + \mathfrak{e}\ddot{\mathcal{S}}(t) - (\mathfrak{f}+\mathfrak{c}+\mathfrak{g}(1-\mathfrak{h}))\ddot{\mathcal{V}}(t)\\
\frac{d\ddot{\mathcal{E}}}{dt} &= \mathfrak{g}\ddot{\mathcal{S}}(t) + \mathfrak{g}(1-\mathfrak{h})\ddot{\mathcal{V}}(t) - (\mathfrak{k}+\mathfrak{f}+\mathfrak{j})\ddot{\mathcal{E}}(t)\\
\frac{d\ddot{\mathcal{I}}}{dt} &= \mathfrak{k}\ddot{\mathcal{E}}(t) - (\mathfrak{f}+\mathfrak{l}+\mathfrak{m})\ddot{\mathcal{I}}(t)\\
\frac{d\ddot{\mathcal{R}}}{dt} &= \mathfrak{j}\ddot{\mathcal{E}}(t) + \mathfrak{m}\ddot{\mathcal{I}}(t) - (\mathfrak{f}+\mathfrak{d}+\mathfrak{n})\ddot{\mathcal{R}}(t)
\end{aligned} \tag{3}$$

The flow chart in Figure 2 provides a systematic overview of the structure of the model. In this section, the pneumonia model is examined using fractal-fractional derivatives, and the model comprises five compartments: Susceptible ($\ddot{\mathcal{S}}$),Vaccinated ($\ddot{\mathcal{V}}$), Exposed ($\ddot{\mathcal{E}}$), Infected ($\ddot{\mathcal{I}}$), and Recovered ($\ddot{\mathcal{R}}$) populations. The total human population is $\ddot{\mathcal{N}}(t) = \ddot{\mathcal{S}}(t) + \ddot{\mathcal{V}}(t) + \ddot{\mathcal{E}}(t) + \ddot{\mathcal{I}}(t) + \ddot{\mathcal{R}}(t)$. The initial conditions are $\ddot{\mathcal{S}}(0) = \ddot{\mathcal{S}}_0$, $\ddot{\mathcal{V}}(0) = \ddot{\mathcal{V}}_0$, $\ddot{\mathcal{E}}(0) = \ddot{\mathcal{E}}_0$, $\ddot{\mathcal{I}}(0) = \ddot{\mathcal{I}}_0$, $\ddot{\mathcal{R}}(0)= \ddot{\mathcal{R}}_0$. The fractal-fractional pneumonia model is formulated as:

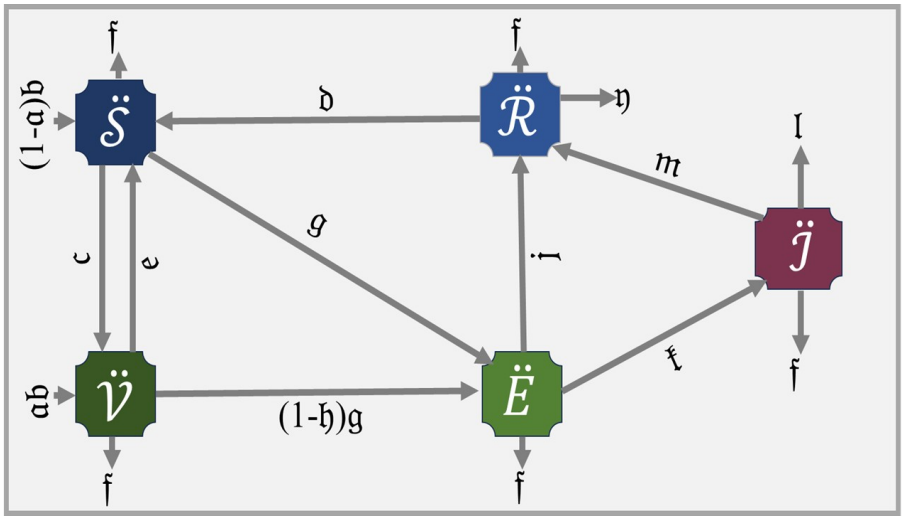

Figure 2: Structure of the Pneumonia Model

$$\begin{aligned}
\mathbb{D}_{\gamma,\rho}(\ddot{\mathcal{S}}(t)) &= (1-\mathfrak{a})\mathfrak{b} + \mathfrak{c}\ddot{\mathcal{V}}(t) + \mathfrak{d}\ddot{\mathcal{R}}(t) - (\mathfrak{e}+\mathfrak{f}+\mathfrak{g})\ddot{\mathcal{S}}(t)\\
\mathbb{D}_{\gamma,\rho}(\ddot{\mathcal{V}}(t)) &= \mathfrak{a}\mathfrak{b} + \mathfrak{e}\ddot{\mathcal{S}}(t) - (\mathfrak{f}+\mathfrak{c}+\mathfrak{g}(1-\mathfrak{h}))\ddot{\mathcal{V}}(t)\\
\mathbb{D}_{\gamma,\rho}(\ddot{\mathcal{E}}(t)) &= \mathfrak{g}\ddot{\mathcal{S}}(t) + \mathfrak{g}(1-\mathfrak{h})\ddot{\mathcal{V}}(t) - (\mathfrak{k}+\mathfrak{f}+\mathfrak{j})\ddot{\mathcal{E}}(t)
\end{aligned}$$

$$\begin{aligned}
\mathbb{D}_{\gamma,\rho}(\ddot{\mathcal{I}}(t)) &= \mathfrak{k}\ddot{\mathcal{E}}(t) - (\mathfrak{f}+\mathfrak{l}+\mathfrak{m})\ddot{\mathcal{I}}(t) \\
\mathbb{D}_{\gamma,\rho}(\ddot{\mathcal{R}}(t)) &= \mathfrak{j}\ddot{\mathcal{E}}(t) + \mathfrak{m}\ddot{\mathcal{I}}(t) - (\mathfrak{f}+\mathfrak{d}+\mathfrak{n})\ddot{\mathcal{R}}(t)
\end{aligned} \tag{4}$$

where $\mathfrak{g} = \frac{\delta\ddot{\mathcal{I}}(t)}{1+\sigma\ddot{\mathcal{I}}(t)}$, γ = fractional order and ρ = fractal order.

The transmission dynamics of *Streptococcus Pneumoniae* are influenced by environmental factors such as seasonal changes and climatic conditions. To better capture this uncertainty, the present study models two critical parameters: the contact rate and the infection rate within the exposed class as fuzzy numbers, which reflect their variability and imprecision. The contact rate δ is treated as a fuzzy number in parametric form, with a central value 0.0287. Similar ambiguity affects the infection rate of exposed individuals $\mathfrak{k}$, which is influenced by inconsistent testing, reporting delays, and variation in incubation periods. To address this, the infection rate is also modelled as a fuzzy parameter, with a central value of 0.01096. The effect of fuzziness of δ and $\mathfrak{k}$ across varying confidence levels is shown in Figure 3 and Figure 4 . By incorporating fuzzy logic through α-cut representation, the model does not rely on exact point estimates. Instead, it captures a range of plausible values for each uncertain parameter, offering a more robust structure for simulation. This is especially useful when the goal is to explore possible outcomes under limited data, rather than to make a single deterministic prediction.
The modified fractal-fractional pneumonia model with fuzzy contact and infected rates is formulated as:

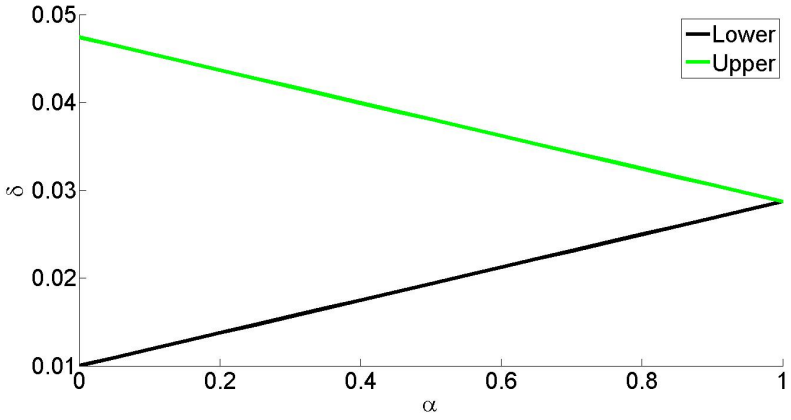

Figure 3: Fuzzy $\tilde{\delta}$ values for different α levels.

$$\begin{aligned}
\mathbb{D}_{\gamma,\rho}(\ddot{\mathcal{S}}(t)) &= [(1\ominus\mathfrak{a})\odot\mathfrak{b}]\oplus[\mathfrak{c}\odot\ddot{\mathcal{V}}(t)]\oplus[\mathfrak{d}\odot\ddot{\mathcal{R}}(t)]\ominus[(\mathfrak{e}\oplus\mathfrak{f}\oplus\tilde{\mathfrak{g}})\odot\ddot{\mathcal{S}}(t)] \\
\mathbb{D}_{\gamma,\rho}(\ddot{\mathcal{V}}(t)) &= [\mathfrak{a}\odot\mathfrak{b}]\oplus[\mathfrak{e}\odot\ddot{\mathcal{S}}(t)]\ominus[(\mathfrak{f}\oplus\mathfrak{c}\oplus\tilde{\mathfrak{g}}\odot(1\ominus\mathfrak{h}))\odot\ddot{\mathcal{V}}(t)] \\
\mathbb{D}_{\gamma,\rho}(\ddot{\mathcal{E}}(t)) &= [\tilde{\mathfrak{g}}\odot\ddot{\mathcal{S}}(t)]\oplus[\tilde{\mathfrak{g}}\odot(1\ominus\mathfrak{h})\odot\ddot{\mathcal{V}}(t)]\ominus[(\tilde{\mathfrak{k}}\oplus\mathfrak{f}\oplus\mathfrak{j})\odot\ddot{\mathcal{E}}(t)] \\
\mathbb{D}_{\gamma,\rho}(\ddot{\mathcal{I}}(t)) &= [\tilde{\mathfrak{k}}\odot\ddot{\mathcal{E}}(t)]\ominus[(\mathfrak{f}\oplus\mathfrak{l}\oplus\mathfrak{m})\odot\ddot{\mathcal{I}}(t)] \\
\mathbb{D}_{\gamma,\rho}(\ddot{\mathcal{R}}(t)) &= [\mathfrak{j}\odot\ddot{\mathcal{E}}(t)]\oplus[\mathfrak{m}\odot\ddot{\mathcal{I}}(t)]\ominus[(\mathfrak{f}\oplus\mathfrak{d}\oplus\mathfrak{n})\odot\ddot{\mathcal{R}}(t)]
\end{aligned} \tag{5}$$

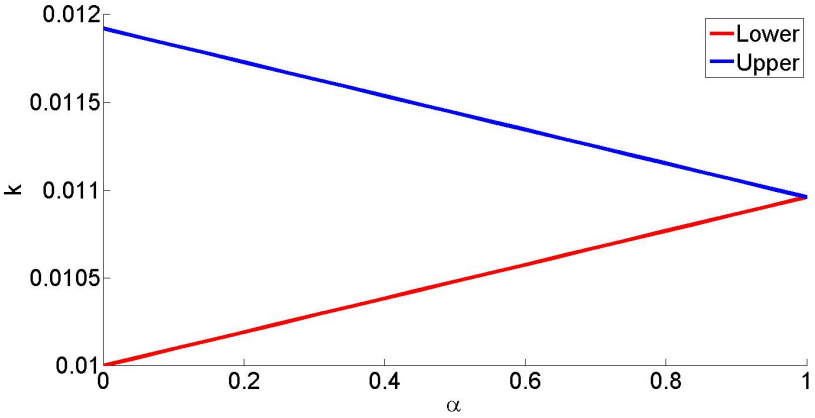

Figure 4: Fuzzy $\tilde{\mathfrak{k}}$ values for different α levels.

where $\tilde{\mathfrak{g}} = \frac{\tilde{\delta}\odot\ddot{\mathcal{I}}(t)}{1\oplus\sigma\odot\ddot{\mathcal{I}}(t)}$, $t \in [0, T]$.

4. Existence and Uniqueness

The mathematical validity of the proposed model requires confirming both the existence and uniqueness of its solutions. In this section, the existence of a solution is valid under continuity and compactness, and it is obtained by Schauder's Fixed Point Theorem[46]. The uniqueness of the solution ensures a single, stable solution when a contractive condition is met, and it is demonstrated using Banach's Fixed Point Theorem. The space of bounded positively solution, $\Delta = \left\{(\ddot{\mathcal{S}}(t),\ \ddot{\mathcal{V}}(t),\ \ddot{\mathcal{E}}(t),\ \ddot{\mathcal{I}}(t),\ \ddot{\mathcal{R}}(t)) \in \mathbb{R}^5_+ \mid 0 \leq \ddot{\mathcal{S}}(t) + \ddot{\mathcal{V}}(t) + \ddot{\mathcal{E}}(t) + \ddot{\mathcal{I}}(t) + \ddot{\mathcal{R}}(t) \leq \frac{\mathfrak{b}}{\mathfrak{f}}\right\}$ with norm $\| \psi \| = \max_{t\in[0,T]} \left(|\ddot{\mathcal{S}}(t)| + |\ddot{\mathcal{V}}(t)| + |\ddot{\mathcal{E}}(t)| + |\ddot{\mathcal{I}}(t)| + |\ddot{\mathcal{R}}(t)|\right)$.
The model (5) becomes,

$$
\begin{aligned}
\varphi_1\big(t,\ddot{\mathcal{S}},\ddot{\mathcal{V}},\ddot{\mathcal{E}},\ddot{\mathcal{I}},\ddot{\mathcal{R}}\big) &= [(1\ominus\mathfrak{a})\odot\mathfrak{b}]\oplus[\mathfrak{c}\odot\ddot{\mathcal{V}}(t)]\oplus[\mathfrak{d}\odot\ddot{\mathcal{R}}(t)]\ominus[(\mathfrak{e}\oplus\mathfrak{f}\oplus\tilde{\mathfrak{g}})\odot\ddot{\mathcal{S}}(t)]\\
\varphi_2\big(t,\ddot{\mathcal{S}},\ddot{\mathcal{V}},\ddot{\mathcal{E}},\ddot{\mathcal{I}},\ddot{\mathcal{R}}\big) &= [\mathfrak{a}\odot\mathfrak{b}]\oplus[\mathfrak{e}\odot\ddot{\mathcal{S}}(t)]\ominus[(\mathfrak{f}\oplus\mathfrak{c}\oplus\tilde{\mathfrak{g}}\odot(1\ominus\mathfrak{h}))\odot\ddot{\mathcal{V}}(t)]\\
\varphi_3\big(t,\ddot{\mathcal{S}},\ddot{\mathcal{V}},\ddot{\mathcal{E}},\ddot{\mathcal{I}},\ddot{\mathcal{R}}\big) &= [\tilde{\mathfrak{g}}\odot\ddot{\mathcal{S}}(t)]\oplus[\tilde{\mathfrak{g}}\odot(1\ominus\mathfrak{h})\odot\ddot{\mathcal{V}}(t)]\ominus[(\tilde{\mathfrak{k}}\oplus\mathfrak{f}\oplus\mathfrak{j})\odot\ddot{\mathcal{E}}(t)]\\
\varphi_4\big(t,\ddot{\mathcal{S}},\ddot{\mathcal{V}},\ddot{\mathcal{E}},\ddot{\mathcal{I}},\ddot{\mathcal{R}}\big) &= [\tilde{\mathfrak{k}}\odot\ddot{\mathcal{E}}(t)]\ominus[(\mathfrak{f}\oplus\mathfrak{l}\oplus\mathfrak{m})\odot\ddot{\mathcal{I}}(t)]\\
\varphi_5\big(t,\ddot{\mathcal{S}},\ddot{\mathcal{V}},\ddot{\mathcal{E}},\ddot{\mathcal{I}},\ddot{\mathcal{R}}\big) &= [\mathfrak{j}\odot\ddot{\mathcal{E}}(t)]\oplus[\mathfrak{m}\odot\ddot{\mathcal{I}}(t)]\ominus[(\mathfrak{f}\oplus\mathfrak{d}\oplus\mathfrak{n})\odot\ddot{\mathcal{R}}(t)]
\end{aligned}
\tag{6}
$$

Fractal-fractional integration(4) implies

$$\ddot{\mathcal{S}}(t) = \ddot{\mathcal{S}}_0 \oplus \frac{(1-\gamma)\rho t^{\rho-1}}{M_{\mathrm{AB}}(\gamma)} \odot \varphi_1\big(t, \ddot{\mathcal{S}}, \ddot{\mathcal{V}}, \ddot{\mathcal{E}}, \ddot{\mathcal{I}}, \ddot{\mathcal{R}}\big) \oplus \frac{\gamma\rho}{M_{\mathrm{AB}}(\gamma)\Gamma(\gamma)} \int_0^t s^{\rho-1}(t-s)^{\gamma-1} \odot \varphi_1\big(s, \ddot{\mathcal{S}}, \ddot{\mathcal{V}}, \ddot{\mathcal{E}}, \ddot{\mathcal{I}}, \ddot{\mathcal{R}}\big) ds$$

$$\ddot{\mathcal{V}}(t) = \ddot{\mathcal{V}}_0 \oplus \frac{(1-\gamma)\rho t^{\rho-1}}{M_{\mathrm{AB}}(\gamma)} \odot \varphi_2\big(t, \ddot{\mathcal{S}}, \ddot{\mathcal{V}}, \ddot{\mathcal{E}}, \ddot{\mathcal{I}}, \ddot{\mathcal{R}}\big) \oplus \frac{\gamma\rho}{M_{\mathrm{AB}}(\gamma)\Gamma(\gamma)} \int_0^t s^{\rho-1}(t-s)^{\gamma-1} \odot \varphi_2\big(s, \ddot{\mathcal{S}}, \ddot{\mathcal{V}}, \ddot{\mathcal{E}}, \ddot{\mathcal{I}}, \ddot{\mathcal{R}}\big) ds$$

$$\ddot{\mathcal{E}}(t) = \ddot{\mathcal{E}}_0 \oplus \frac{(1-\gamma)\rho t^{\rho-1}}{M_{\mathrm{AB}}(\gamma)} \odot \varphi_3\big(t, \ddot{\mathcal{S}}, \ddot{\mathcal{V}}, \ddot{\mathcal{E}}, \ddot{\mathcal{I}}, \ddot{\mathcal{R}}\big) \oplus \frac{\gamma\rho}{M_{\mathrm{AB}}(\gamma)\Gamma(\gamma)} \int_0^t s^{\rho-1}(t-s)^{\gamma-1} \odot \varphi_3\big(s, \ddot{\mathcal{S}}, \ddot{\mathcal{V}}, \ddot{\mathcal{E}}, \ddot{\mathcal{I}}, \ddot{\mathcal{R}}\big) ds$$

$$\ddot{\mathcal{I}}(t) = \ddot{\mathcal{I}}_0 \oplus \frac{(1-\gamma)\rho t^{\rho-1}}{M_{\mathrm{AB}}(\gamma)} \odot \varphi_4\big(t, \ddot{\mathcal{S}}, \ddot{\mathcal{V}}, \ddot{\mathcal{E}}, \ddot{\mathcal{I}}, \ddot{\mathcal{R}}\big) \oplus \frac{\gamma\rho}{M_{\mathrm{AB}}(\gamma)\Gamma(\gamma)} \int_0^t s^{\rho-1}(t-s)^{\gamma-1} \odot \varphi_4\big(s, \ddot{\mathcal{S}}, \ddot{\mathcal{V}}, \ddot{\mathcal{E}}, \ddot{\mathcal{I}}, \ddot{\mathcal{R}}\big) ds$$

$$\ddot{\mathcal{R}}(t) = \ddot{\mathcal{R}}_0 \oplus \frac{(1-\gamma)\rho t^{\rho-1}}{M_{\mathrm{AB}}(\gamma)} \odot \varphi_5\big(t, \ddot{\mathcal{S}}, \ddot{\mathcal{V}}, \ddot{\mathcal{E}}, \ddot{\mathcal{I}}, \ddot{\mathcal{R}}\big) \oplus \frac{\gamma\rho}{M_{\mathrm{AB}}(\gamma)\Gamma(\gamma)} \int_0^t s^{\rho-1}(t-s)^{\gamma-1} \odot \varphi_5\big(s, \ddot{\mathcal{S}}, \ddot{\mathcal{V}}, \ddot{\mathcal{E}}, \ddot{\mathcal{I}}, \ddot{\mathcal{R}}\big) ds$$

The generalized system is represented as

$$\begin{aligned} \mathbb{D}_{\gamma,\rho}\big(\chi(t)\big) &= \eth\big(t, \chi(t)\big) \\ \chi(0) &= \chi_0 \end{aligned} \tag{7}$$

$$\chi(t) = \chi_0 \oplus \frac{(1-\gamma)\rho t^{\rho-1}}{M_{\mathrm{AB}}(\gamma)} \odot \eth\big(t, \chi(t)\big) \oplus \frac{\gamma\rho}{M_{\mathrm{AB}}(\gamma)\Gamma(\gamma)} \int_0^t s^{\rho-1}(t-s)^{\gamma-1} \odot \eth\big(s, \chi(s)\big) ds \tag{8}$$

where $\chi(t) = \begin{pmatrix} \ddot{\mathcal{S}} \\ \ddot{\mathcal{V}} \\ \ddot{\mathcal{E}} \\ \ddot{\mathcal{I}} \\ \ddot{\mathcal{R}} \end{pmatrix}$ and the fuzzy valued function $\eth\big(t, \chi(t)\big) = \begin{pmatrix} \varphi_1\big(t, \ddot{\mathcal{S}}, \ddot{\mathcal{V}}, \ddot{\mathcal{E}}, \ddot{\mathcal{I}}, \ddot{\mathcal{R}}\big) \\ \varphi_2\big(t, \ddot{\mathcal{S}}, \ddot{\mathcal{V}}, \ddot{\mathcal{E}}, \ddot{\mathcal{I}}, \ddot{\mathcal{R}}\big) \\ \varphi_3\big(t, \ddot{\mathcal{S}}, \ddot{\mathcal{V}}, \ddot{\mathcal{E}}, \ddot{\mathcal{I}}, \ddot{\mathcal{R}}\big) \\ \varphi_4\big(t, \ddot{\mathcal{S}}, \ddot{\mathcal{V}}, \ddot{\mathcal{E}}, \ddot{\mathcal{I}}, \ddot{\mathcal{R}}\big) \\ \varphi_5\big(t, \ddot{\mathcal{S}}, \ddot{\mathcal{V}}, \ddot{\mathcal{E}}, \ddot{\mathcal{I}}, \ddot{\mathcal{R}}\big) \end{pmatrix}$.

An operator $\Psi : \Delta \to \Delta$ defined as

$$\Psi\big(\chi(t)\big) = \chi_0 \oplus \frac{(1-\gamma)\rho t^{\rho-1}}{M_{\mathrm{AB}}(\gamma)} \odot \eth\big(t, \chi\big) \oplus \frac{\gamma\rho}{M_{\mathrm{AB}}(\gamma)\Gamma(\gamma)} \int_0^t s^{\rho-1}(t-s)^{\gamma-1} \odot \eth\big(s, \chi\big) ds$$

To find the existence of the considered model, Schaefer's fixed point theorem was used. The theorem implies that Ψ has at least one fixed point if

[**I**] $\lambda(\Psi) = \Big\{\chi \in \Delta \mid \chi = \alpha\Psi(\chi),\ 0 \le \alpha \le 1\Big\}$ is a bounded set.

[**II**] The operator Ψ is completely continuous.

Theorem 1. ***[Existence]*** *The proposed system has unique solution if [I] and [II] holds.*

Proof. To prove that $\eth\big(t, \chi(t)\big)$ satisfies the Lipschitz condition.
Let $\chi, \kappa \in \Delta$.
(i) For φ_1,

$$\varrho\Big(\varphi_1\big(t, \ddot{\mathcal{S}}_1, \ddot{\mathcal{V}}, \ddot{\mathcal{E}}, \ddot{\mathcal{I}}, \ddot{\mathcal{R}}\big), \varphi_1\big(t, \ddot{\mathcal{S}}_2, \ddot{\mathcal{V}}, \ddot{\mathcal{E}}, \ddot{\mathcal{I}}, \ddot{\mathcal{R}}\big)\Big) \le \mathcal{Y}_s^{\varphi_1} \varrho\Big(\ddot{\mathcal{S}}_1, \ddot{\mathcal{S}}_2\Big)$$

with $\mathcal{Y}_s^{\varphi_1} = |\mathfrak{e} + \mathfrak{f} + \tilde{\mathfrak{g}}|$,

$$\varrho\Big(\varphi_1\big(t, \ddot{\mathcal{S}}, \ddot{\mathcal{V}}_1, \ddot{\mathcal{E}}, \ddot{\mathcal{I}}, \ddot{\mathcal{R}}\big), \varphi_1\big(t, \ddot{\mathcal{S}}, \ddot{\mathcal{V}}_2, \ddot{\mathcal{E}}, \ddot{\mathcal{I}}, \ddot{\mathcal{R}}\big)\Big) \leq \mathcal{Y}_v^{\varphi_1} \varrho\Big(\ddot{\mathcal{V}}_1, \ddot{\mathcal{V}}_2\Big)$$

with $\mathcal{Y}_v^{\varphi_1} = |\mathfrak{c}|$.

$$\varrho\Big(\varphi_1\big(t, \ddot{\mathcal{S}}, \ddot{\mathcal{V}}, \ddot{\mathcal{E}}, \ddot{\mathcal{I}}, \ddot{\mathcal{R}}_1\big), \varphi_1\big(t, \ddot{\mathcal{S}}, \ddot{\mathcal{V}}, \ddot{\mathcal{E}}, \ddot{\mathcal{I}}, \ddot{\mathcal{R}}_2\big)\Big) \leq \mathcal{Y}_v^{\varphi_1} \varrho\Big(\ddot{\mathcal{R}}_1 - \ddot{\mathcal{R}}_2\Big)$$

with $\mathcal{Y}_r^{\varphi_1} = |\mathfrak{d}|$.
Let $\mathcal{Y}^{\varphi_1} = \max\Big\{\mathcal{Y}_s^{\varphi_1}, \mathcal{Y}_v^{\varphi_1}, \mathcal{Y}_r^{\varphi_1}\Big\}$

$$\therefore \varrho\Big(\varphi_1\big(t, \chi(t)\big), \varphi_1\big(t, \kappa(t)\big)\Big) \leq \mathcal{Y}^{\varphi_1} \varrho\Big(\chi(t), \kappa(t)\Big)$$

(ii) For φ_2, $\mathcal{Y}_s^{\varphi_2} = |\mathfrak{e}|$, $\mathcal{Y}_v^{\varphi_2} = |\mathfrak{f} + \mathfrak{c} + \tilde{\mathfrak{g}}(1 - \mathfrak{h})|$ and $\mathcal{Y}^{\varphi_2} = \max\Big\{\mathcal{Y}_s^{\varphi_2}, \mathcal{Y}_v^{\varphi_2}\Big\}$.

$$\therefore \varrho\Big(\varphi_2\big(t, \chi(t)\big), \varphi_2\big(t, \kappa(t)\big)\Big) \leq \mathcal{Y}^{\varphi_2} \varrho\Big(\chi(t), \kappa(t)\Big)$$

(iii) For φ_3, $\mathcal{Y}_s^{\varphi_3} = |\tilde{\mathfrak{g}}|$, $\mathcal{Y}_v^{\varphi_3} = |\tilde{\mathfrak{g}}(1 - \mathfrak{h})|$, $\mathcal{Y}_e^{\varphi_3} = |\mathfrak{f} + \mathfrak{j} + \tilde{\mathfrak{k}}|$ and $\mathcal{Y}^{\varphi_3} = \max\Big\{\mathcal{Y}_s^{\varphi_3}, \mathcal{Y}_v^{\varphi_3}, \mathcal{Y}_e^{\varphi_3}\Big\}$

$$\therefore \varrho\Big(\varphi_3\big(t, \chi(t)\big), \varphi_3\big(t, \kappa(t)\big)\Big) \leq \mathcal{Y}^{\varphi_3} \varrho\Big(\chi(t), \kappa(t)\Big)$$

(iv) For φ_4,$\mathcal{Y}_e^{\varphi_4} = |\tilde{\mathfrak{k}}|$, $\mathcal{Y}_i^{\varphi_4} = |\mathfrak{f} + \mathfrak{l} + \mathfrak{m}|$ and $\mathcal{Y}^{\varphi_4} = \max\Big\{\mathcal{Y}_e^{\varphi_4}, \mathcal{Y}_i^{\varphi_4}\Big\}$.

$$\therefore \varrho\Big(\varphi_4\big(t, \chi(t)\big), \varphi_4\big(t, \kappa(t)\big)\Big) \leq \mathcal{Y}^{\varphi_4} \varrho\Big(\chi(t), \kappa(t)\Big)$$

(v) For φ_5, $\mathcal{Y}_e^{\varphi_5} = |\mathfrak{j}|$, $\mathcal{Y}_i^{\varphi_5} = |\mathfrak{m}|$, $\mathcal{Y}_r^{\varphi_5} = |\mathfrak{f} + \mathfrak{d} + \mathfrak{n}|$ and $\mathcal{Y}^{\varphi_5} = \max\Big\{\mathcal{Y}_e^{\varphi_5}, \mathcal{Y}_i^{\varphi_5}, \mathcal{Y}_r^{\varphi_5}\Big\}$

$$\therefore \varrho\Big(\varphi_3\big(t, \chi(t)\big), \varphi_3\big(t, \kappa(t)\big)\Big) \leq \mathcal{Y}^{\varphi_3} \varrho\Big(\chi(t), \kappa(t)\Big)$$

Hence, $\varphi_1, \varphi_2, \varphi_3, \varphi_4, \varphi_5$ satisfies the Lipschitz condition.
Consider $\mathcal{Y} = \max\Big\{\mathcal{Y}^{\varphi_1}, \mathcal{Y}^{\varphi_2}, \mathcal{Y}^{\varphi_3}, \mathcal{Y}^{\varphi_4}, \mathcal{Y}^{\varphi_5}\Big\}$, then for $\chi, \kappa \in \Delta$

$$\varrho\Big(\eth\big(t, \chi(t)\big), \eth\big(t, \kappa(t)\big)\Big) \leq \mathcal{Y} \varrho\Big(\chi(t), \kappa(t)\Big) \tag{9}$$

Hence $\eth\big(t, \chi\big)$ satisfies the Lipschitz condition.
Assume that a sequence of $\{\chi_n\}$ converges to χ in Δ.

$$\Big\|\Psi\Big(\chi_n\Big) - \Psi\Big(\chi\Big)\Big\| \leq \max_{t \in [0,T]} \left(\frac{(1-\gamma)\rho t^{\rho-1}}{M_{\mathrm{AB}}(\gamma)} \varrho\Big(\eth\big(t, \chi_n(t)\big), \eth\big(t, \chi(t)\big)\Big) \right.$$

$$+\frac{\gamma\rho}{M_{\mathrm{AB}}(\gamma)\Gamma(\gamma)}\int_0^t s^{\rho-1}(t-s)^{\gamma-1}\varrho\Big(\Im\big(s,\chi_n(s)\big),\Im\big(s,\chi(s)\big)\Big)ds\Bigg)$$

$$\leq \frac{(1-\gamma)\rho T^{\rho-1}}{M_{\mathrm{AB}}(\gamma)}\mathcal{Y}\varrho\big(\chi_n,\chi\big)+\frac{\gamma\rho}{M_{\mathrm{AB}}(\gamma)\Gamma(\gamma)}\mathcal{Y}\varrho\big(\chi_n,\chi\big)\max_{t\in[0,T]}\int_0^t s^{\rho-1}(t-s)^{\gamma-1}ds$$

Since $\int_0^t s^{\rho-1}(t-s)^{\gamma-1}ds=\int_0^1 t^{\gamma+\rho-1}z^{\rho-1}(1-z)^{\gamma-1}dz$ by taking $s=tz$.
Substituting Beta function $B(\gamma,\rho)$,

$$\Big\|\Psi\Big(\chi_n\Big)-\Psi\Big(\chi\Big)\Big\|\leq\left[\frac{(1-\gamma)\rho T^{\rho-1}}{M_{\mathrm{AB}}(\gamma)}+\frac{\gamma\rho T^{\gamma+\rho-1}}{M_{\mathrm{AB}}(\gamma)\Gamma(\gamma)}B(\gamma,\rho)\right]\odot\mathcal{Y}\varrho\big(\chi_n,\chi\big)$$

$$\Big\|\Psi\Big(\chi_n\Big)-\Psi\Big(\chi\Big)\Big\|\leq\xi\mathcal{Y}\odot\varrho\big(\chi_n,\chi\big)\tag{10}$$

where $\xi=\left[\frac{(1-\gamma)\rho T^{\rho-1}}{M_{\mathrm{AB}}(\gamma)}+\frac{\gamma\rho T^{\gamma+\rho-1}}{M_{\mathrm{AB}}(\gamma)\Gamma(\gamma)}B(\gamma,\rho)\right]$.
Hence $\Psi\Big(\chi_n\Big)\to\Psi\Big(\chi\Big)$ whenever $\{\chi_n\}\to\chi$ as n tends to ∞.
$\therefore\ \Psi$ is continuous.
For a bounded set χ of Δ, there is a bound ϑ.
For all χ, $\Big\|\Psi\Big(\chi\Big)\Big\|\leq\xi\ \vartheta$.
$\therefore\ \Psi$ is uniformly bounded.
For $t,z\in[0,T]$,

$$\Big\|\Psi\Big(\chi(t)\Big)-\Psi\Big(\chi(z)\Big)\Big\|\leq\left[\frac{(1-\gamma)\rho}{M_{\mathrm{AB}}(\gamma)}\vartheta\right]\big(t^{\rho-1}-z^{\rho-1}\big)$$
$$+\left[\frac{(1-\gamma)\rho T^{\rho-1}}{M_{\mathrm{AB}}(\gamma)}+\frac{\gamma\rho\vartheta}{M_{\mathrm{AB}}(\gamma)\Gamma(\gamma)}B(\gamma,\rho)\right]\big(t^{\gamma+\rho-1}-z^{\gamma+\rho-1}\big)$$

$\therefore\ \Big\|\Psi\Big(\chi(t)\Big)-\Psi\Big(\chi(z)\Big)\Big\|\to 0$ as $t\to z$. Then, Ψ is uniformly continuous.
Arzela-Ascoli theorem implies that Ψ is equicontinuous and relatively compact.
$\therefore\ \Psi$ is completely continuous. Hence, [I] holds
Let $\kappa\in\lambda(\Psi)$. Then $\|\kappa\|=\|\alpha\Psi(\chi)\|\leq\xi\ \vartheta$.
Hence, [II] holds.
$\therefore\ \Psi$ has atleast one fixed point.

Theorem 2. ***[Uniqueness]*** *If $\xi\mathcal{Y}<1$, then the system (5) has unique solution.*

Proof. Let $\Theta_\chi=\max\limits_{t\in[0,T]}\varrho\Big(\Im(t,0),0\Big)<\infty$ such that $\xi\big(\mathcal{Y}\mathcal{A}+\Theta_\chi\big)\leq\mathcal{A}$.
Assume that $\mathscr{G}_{\mathcal{A}}=\big\{\chi\in\Delta:\|\chi\|\leq\mathcal{A}\big\}$. To verify that $\Psi(\mathscr{G}_{\mathcal{A}})\subset\mathscr{G}_{\mathcal{A}}$.

$$\|\Psi(\chi)\|\leq\max_{t\in[0,T]}\left(\frac{(1-\gamma)\rho t^{\rho-1}}{M_{\mathrm{AB}}(\gamma)}\left[\varrho\Big(\Im\big(t,\chi(t)\big),\Im\big(t,0\big)\Big)+\varrho\Big(\Im\big(t,0\big),0\Big)\right]\right.$$

$$+\frac{\gamma\rho}{M_{\mathrm{AB}}(\gamma)\Gamma(\gamma)}\int_0^t s^{\rho-1}(t-s)^{\gamma-1}\left[\varrho\Big(\eth\big(t,\chi(t)\big),\eth\big(t,0\big)\Big)+\varrho\Big(\eth\big(t,0\big),0\Big)\right]ds\Bigg)$$

$$\begin{aligned}\therefore \|\Psi(\chi)\| &\le \xi\big(\mathcal{Y}\,\|\chi\|+\Theta_\chi\big)\\ &\le \xi\big(\mathcal{Y}\mathcal{A}+\Theta_\chi\big)\\ &\le \mathcal{A}\end{aligned}$$

Hence $\|\Psi(\chi)\| \le \mathcal{A}$, $\forall\ \chi \in \mathscr{G}_{\mathcal{A}}$.
$\therefore \|\Psi(\chi)-\Psi(\kappa)\| \le \xi\mathcal{Y}\varrho(\chi-\kappa)$, $\forall\ \chi,\kappa \in \Delta$ and $t \in [0,T]$
Since, $\xi\mathcal{Y} < 1$, then the operator Ψ possess contraction.
Banach fixed point theorem verifies that the system (5) has unique solution.

5. Ulam-Hyers Stability

This section reveals how sensitive the model's results are to slight adjustments in parameters or initial conditions. The Ulam-Hyers stability. confirms that approximate solutions stay close to the exact solution when small deviations occur.
Consider a small change perturbation by Φ on the system 7 such that $\Phi(0)=0$ and $\big|\Phi(t)\big| \le \sigma$.
The system

$$\begin{aligned}\mathbb{D}_{\gamma,\rho}\big(\chi(t)\big) &= \eth\big(t,\chi(t)\big)\oplus\Phi(t)\\ \chi(0) &= \chi_0\end{aligned}\tag{11}$$

Lemma 1. *The system (11) satisfies*

$$\left|\chi(t)\ominus\Big(\chi_0\oplus\tfrac{(1-\gamma)\rho t^{\rho-1}}{M_{\mathrm{AB}}(\gamma)}\odot\eth\big(t,\chi(t)\big)\oplus\tfrac{\gamma\rho}{M_{\mathrm{AB}}(\gamma)\Gamma(\gamma)}\textstyle\int_0^t s^{\rho-1}(t-s)^{\gamma-1}\odot\eth\big(s,\chi(s)\big)ds\Big)\right| \le (\xi\sigma).\tag{12}$$

Proof. Equation (8) and $\big|\Phi(t)\big| \le \sigma$ implies the solution (12).

Theorem 3. *If $(\xi\mathcal{Y}) \le 1$ and Lemma 1 holds, then the system is Ulam-Hyers stable.*

Proof. For $t \in [0,T]$,

$$\big|\chi(t)\ominus\kappa(t)\big| = \left|\chi(t)\ominus\left(\kappa_0\oplus\tfrac{(1-\gamma)\rho t^{\rho-1}}{M_{\mathrm{AB}}(\gamma)}\odot\eth\big(t,\kappa(t)\big)\oplus\tfrac{\gamma\rho}{M_{\mathrm{AB}}(\gamma)\Gamma(\gamma)}\textstyle\int_0^t s^{\rho-1}(t-s)^{\gamma-1}\odot\eth\big(s,\kappa(s)\big)ds\right)\right|$$

$$\le \left|\chi(t)\ominus\left(\chi_0\oplus\frac{(1-\gamma)\rho t^{\rho-1}}{M_{\mathrm{AB}}(\gamma)}\odot\eth\big(t,\chi(t)\big)\oplus\frac{\gamma\rho}{M_{\mathrm{AB}}(\gamma)\Gamma(\gamma)}\int_0^t s^{\rho-1}(t-s)^{\gamma-1}\odot\eth\big(s,\chi(s)\big)ds\right)\right|$$
$$\oplus\left|\left(\chi_0\oplus\frac{(1-\gamma)\rho t^{\rho-1}}{M_{\mathrm{AB}}(\gamma)}\odot\eth\big(t,\chi(t)\big)\oplus\frac{\gamma\rho}{M_{\mathrm{AB}}(\gamma)\Gamma(\gamma)}\int_0^t s^{\rho-1}(t-s)^{\gamma-1}\odot\eth\big(s,\chi(s)\big)ds\right)\right.$$

$$\ominus\left(\kappa_0+\frac{(1-\gamma)\rho t^{\rho-1}}{M_{\mathrm{AB}}(\gamma)}\odot\eth\big(t,\kappa(t)\big)\oplus\frac{\gamma\rho}{M_{\mathrm{AB}}(\gamma)\Gamma(\gamma)}\int_0^t s^{\rho-1}(t-s)^{\gamma-1}\odot\eth\big(s,\kappa(s)\big)ds\right)\Bigg|$$

$$\leq(\xi\sigma)+(\xi\mathcal{Y})\,\|\chi-\kappa\|$$

$$\therefore\|\chi-\kappa\|\leq\left(\frac{\xi}{1-(\xi\mathcal{Y})}\right)\sigma=\mathfrak{C}\sigma$$

Hence, the system is Ulam-Hyers stable.

6. Results and Discussions

In this section, the system is solved using the Lagrange piecewise interpolation method and the results obtained from the MATLAB software simulations. The solution of the system (5) is

$$[\tilde{\ddot{\mathcal{S}}}(t_{i+1})]_\alpha=[\tilde{\ddot{\mathcal{S}}}_0]_\alpha\oplus\frac{(1-\gamma)\rho t_i^{\rho-1}}{M_{\mathrm{AB}}(\gamma)}\odot\varphi_1\big(t_i,\ddot{\mathcal{S}},\ddot{\mathcal{V}},\ddot{\mathcal{E}},\ddot{\mathcal{I}},\ddot{\mathcal{R}}\big)\oplus\frac{\rho k^\gamma}{M_{\mathrm{AB}}(\gamma)\Gamma(\gamma+2)}$$
$$\odot\sum_{n=0}^{i}\Bigg[t_n^{\rho-1}\odot\varphi_1\big(t_n,\ddot{\mathcal{S}},\ddot{\mathcal{V}},\ddot{\mathcal{E}},\ddot{\mathcal{I}},\ddot{\mathcal{R}}\big)\Big((i+1-n)^\gamma(i-n+2+\gamma)-(i-n)^\gamma(i-n+2+2\gamma)\Big)$$
$$\ominus t_{n-1}^{\rho-1}\odot\varphi_1\big(t_{n-1},\ddot{\mathcal{S}},\ddot{\mathcal{V}},\ddot{\mathcal{E}},\ddot{\mathcal{I}},\ddot{\mathcal{R}}\big)\Big((i-n+1)^{\gamma+1}-(i-n)^\gamma(i-n+1+\gamma)\Big)\Bigg]$$

$$[\tilde{\ddot{\mathcal{V}}}(t_{j+1})]_\alpha=[\tilde{\ddot{\mathcal{V}}}_0]_\alpha\oplus\frac{(1-\gamma)\rho t_i^{\rho-1}}{M_{\mathrm{AB}}(\gamma)}\odot\varphi_2\big(t_i,\ddot{\mathcal{S}},\ddot{\mathcal{V}},\ddot{\mathcal{E}},\ddot{\mathcal{I}},\ddot{\mathcal{R}}\big)\oplus\frac{\rho k^\rho}{M_{\mathrm{AB}}(\gamma)\Gamma(\gamma+2)}$$
$$\odot\sum_{n=0}^{i}\Bigg[t_n^{\rho-1}\odot\varphi_2\big(t_n,\ddot{\mathcal{S}},\ddot{\mathcal{V}},\ddot{\mathcal{E}},\ddot{\mathcal{I}},\ddot{\mathcal{R}}\big)\Big((i+1-n)^\gamma(i-n+2+\gamma)-(i-n)^\gamma(i-n+2+2\gamma)\Big)$$
$$\ominus t_{n-1}^{\rho-1}\odot\varphi_2\big(t_{n-1},\ddot{\mathcal{S}},\ddot{\mathcal{V}},\ddot{\mathcal{E}},\ddot{\mathcal{I}},\ddot{\mathcal{R}}\big)\Big((i-n+1)^{\gamma+1}-(i-n)^\gamma(i-n+1+\gamma)\Big)\Bigg]$$

$$[\tilde{\ddot{\mathcal{E}}}(t_{i+1})]_\alpha=[\tilde{\ddot{\mathcal{E}}}_0]_\alpha\oplus\frac{(1-\gamma)\rho t_i^{\rho-1}}{M_{\mathrm{AB}}(\gamma)}\odot\varphi_3\big(t_i,\ddot{\mathcal{S}},\ddot{\mathcal{V}},\ddot{\mathcal{E}},\ddot{\mathcal{I}},\ddot{\mathcal{R}}\big)\oplus\frac{\rho k^\gamma}{M_{\mathrm{AB}}(\gamma)\Gamma(\gamma+2)}$$
$$\odot\sum_{n=0}^{i}\Bigg[t_n^{\rho-1}\odot\varphi_3\big(t_n,\ddot{\mathcal{S}},\ddot{\mathcal{V}},\ddot{\mathcal{E}},\ddot{\mathcal{I}},\ddot{\mathcal{R}}\big)\Big((i+1-n)^\gamma(i-n+2+\gamma)-(i-n)^\gamma(i-n+2+2\gamma)\Big)$$
$$\ominus t_{n-1}^{\rho-1}\odot\varphi_3\big(t_{n-1},\ddot{\mathcal{S}},\ddot{\mathcal{V}},\ddot{\mathcal{E}},\ddot{\mathcal{I}},\ddot{\mathcal{R}}\big)\Big((i-n+1)^{\gamma+1}-(i-n)^\gamma(i-n+1+\gamma)\Big)\Bigg]$$

$$[\tilde{\ddot{\mathcal{I}}}(t_{i+1})]_\alpha=[\tilde{\ddot{\mathcal{I}}}_0]_\alpha\oplus\frac{(1-\gamma)\rho t_i^{\rho-1}}{M_{\mathrm{AB}}(\gamma)}\odot\varphi_4\big(t_i,\ddot{\mathcal{S}},\ddot{\mathcal{V}},\ddot{\mathcal{E}},\ddot{\mathcal{I}},\ddot{\mathcal{R}}\big)\oplus\frac{\rho k^\gamma}{M_{\mathrm{AB}}(\gamma)\Gamma(\gamma+2)}$$
$$\odot\sum_{n=0}^{i}\Bigg[t_n^{\rho-1}\odot\varphi_4\big(t_n,\ddot{\mathcal{S}},\ddot{\mathcal{V}},\ddot{\mathcal{E}},\ddot{\mathcal{I}},\ddot{\mathcal{R}}\big)\Big((i+1-n)^\gamma(i-n+2+\gamma)-(i-n)^\gamma(i-n+2+2\gamma)\Big)$$

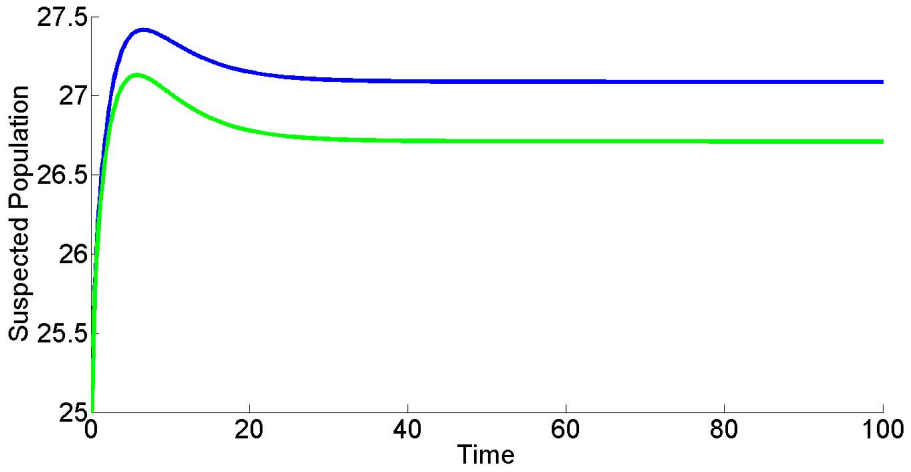

Figure 5: Fuzzy susceptiple population over time

$$\ominus\, t_{n-1}^{\rho-1} \odot \varphi_4\big(t_{n-1}, \ddot{\mathcal{S}}, \ddot{\mathcal{V}}, \ddot{\mathcal{E}}, \ddot{\mathcal{I}}, \ddot{\mathcal{R}}\big)\Big((i-n+1)^{\gamma+1} - (i-n)^{\gamma}(i-n+1+\gamma)\Big)\Bigg]$$

$$[\ddot{\tilde{\mathcal{R}}}(t_{i+1})]_\alpha = [\ddot{\tilde{\mathcal{R}}}_0]_\alpha \oplus \frac{(1-\gamma)\rho t_i^{\rho-1}}{M_{\mathrm{AB}}(\gamma)} \odot \varphi_5\big(t_i, \ddot{\mathcal{S}}, \ddot{\mathcal{V}}, \ddot{\mathcal{E}}, \ddot{\mathcal{I}}, \ddot{\mathcal{R}}\big) \oplus \frac{\rho k^{\gamma}}{M_{\mathrm{AB}}(\gamma)\Gamma(\gamma+2)}$$
$$\odot \sum_{n=0}^{i} \Bigg[t_n^{\rho-1} \odot \varphi_5\big(t_n, \ddot{\mathcal{S}}, \ddot{\mathcal{V}}, \ddot{\mathcal{E}}, \ddot{\mathcal{I}}, \ddot{\mathcal{R}}\big)\Big((i+1-n)^{\gamma}(i-n+2+\gamma) - (i-n)^{\gamma}(i-n+2+2\gamma)\Big)$$
$$\ominus\, t_{n-1}^{\rho-1} \odot \varphi_5\big(t_{n-1}, \ddot{\mathcal{S}}, \ddot{\mathcal{V}}, \ddot{\mathcal{E}}, \ddot{\mathcal{I}}, \ddot{\mathcal{R}}\big)\Big((i-n+1)^{\gamma+1} - (i-n)^{\gamma}(i-n+1+\gamma)\Big)\Bigg] \tag{13}$$

To study the behavior of the proposed fuzzy fractal–fractional pneumonia model, numerical simulations were carried out over the time interval $t \in [0, 100]$. The model was solved using the Lagrange piecewise interpolation, and the integral limits were partitioned into 'i' with difference k and then the results obtained with $\gamma = 0.99$, $\rho = 0.98$ and fuzzy level $(\alpha) = 0$. The fractional order captures the memory effect inherent in the progression and control of infectious diseases like pneumonia. This accounts for the influence of past states on current dynamics, which is particularly relevant in cases of immunity, delayed symptoms, or gradual recovery. The fractal dimension was selected to incorporate the non-smooth, irregular interactions within populations, such as inconsistent contact patterns and irregular immune responses, which are not well-represented in classical models. Although these values were assumed for this theoretical study, they can be adjusted and calibrated using real clinical or population data in future applications to reflect more accurate disease dynamics. Once actual data are available, the model can be simulated using optimized values of the fractal and fractional dimensions, improving its relevance and predictive power.

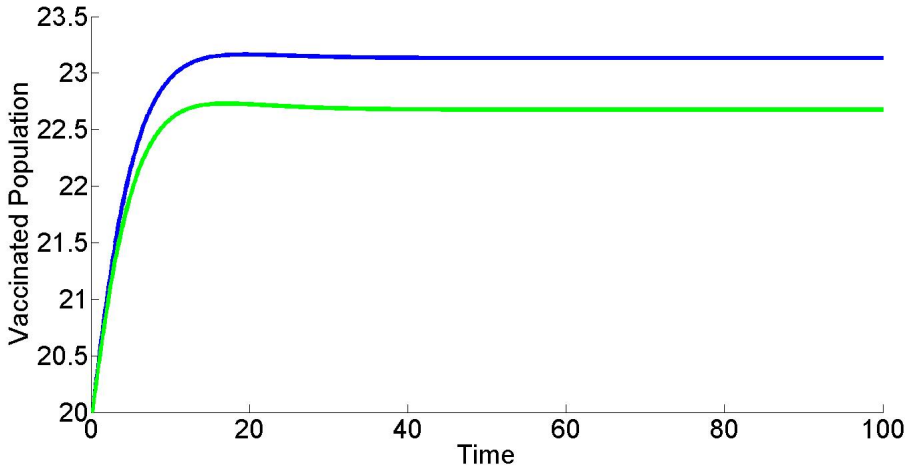

Figure 6: Fuzzy vaccinated population over time

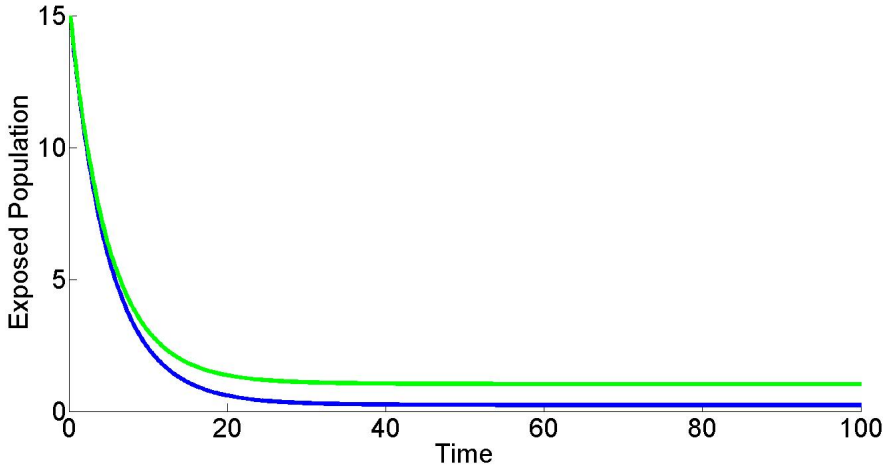

Figure 7: Fuzzy exposed population over time

Susceptible Population: Figure 5 captures the dynamics of the suspectible class. The population rises briefly in the early stage due to active case detection, peaking around time $t = 10$, then gradually stabilizes. The population settles between 26 and 27.5, suggesting that early surveillance and monitoring play a key role in controlling the outbreak before it escalates.

Vaccinated Population: In Figure 6, the vaccinated population demonstrates a monotonic increase within the first 20 time units and stabilizing slightly above 23. This trend confirms sustained and effective vaccination implementation over time. The observed fuzzy band between solution curves reflects uncertainty in vaccination efficacy or uptake rate but remains stable, ensuring the reliability of long-term predictions.

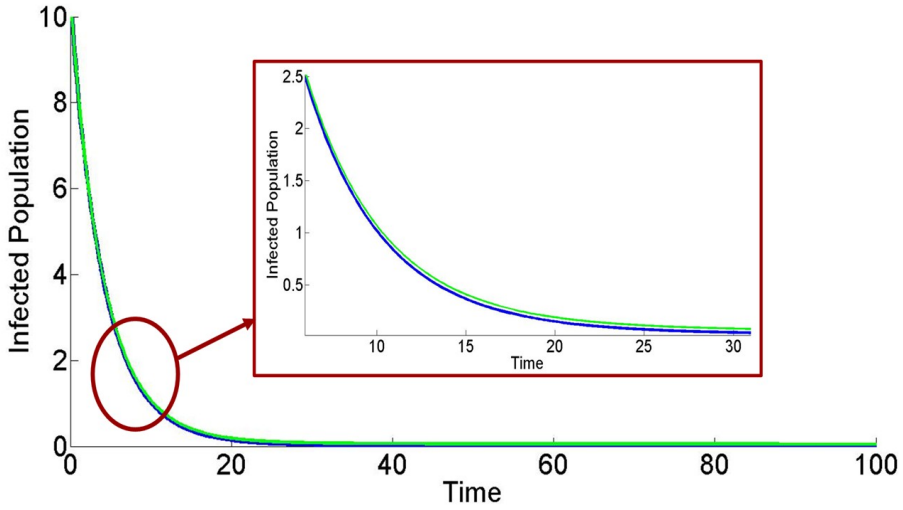

Figure 8: Fuzzy infected population over time

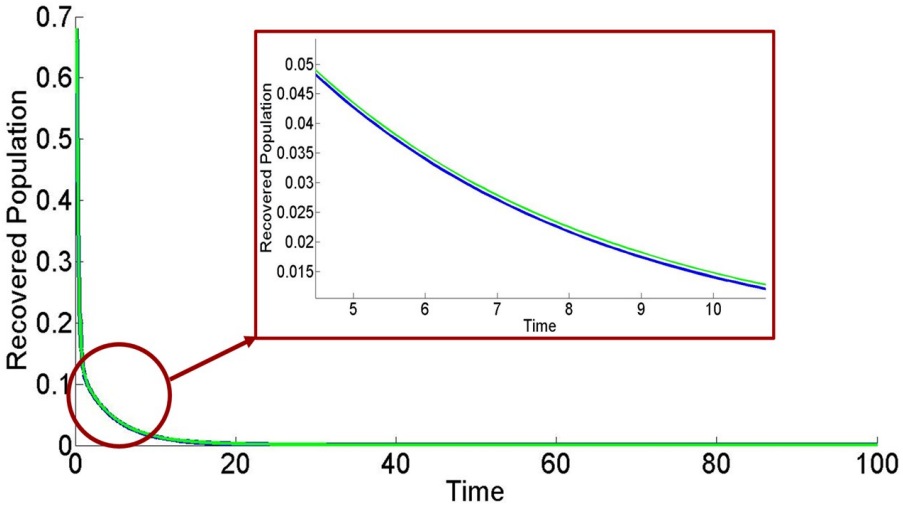

Figure 9: Fuzzy recovery population over time

Exposed Population: The exposed class, Figure 7 shows a similar decline within the first 15 time units and approaching near-zero levels by time t=30. This indicates that potential cases either move to the infected class or are neutralized due to preventive measures. The gap between the fuzzy solutions is slightly wider in this compartment, emphasizing that uncertainty in incubation or exposure response rates can influence early-stage predictions.

Infected Population: The infected class shown in Figure 8 exhibits a steep initial decline. Starting from around 10, the population falls below 1 within the first 20 time units and trends toward zero afterward. This rapid decay highlights the combined effectiveness of vaccination and natural recovery in curbing active infections. The

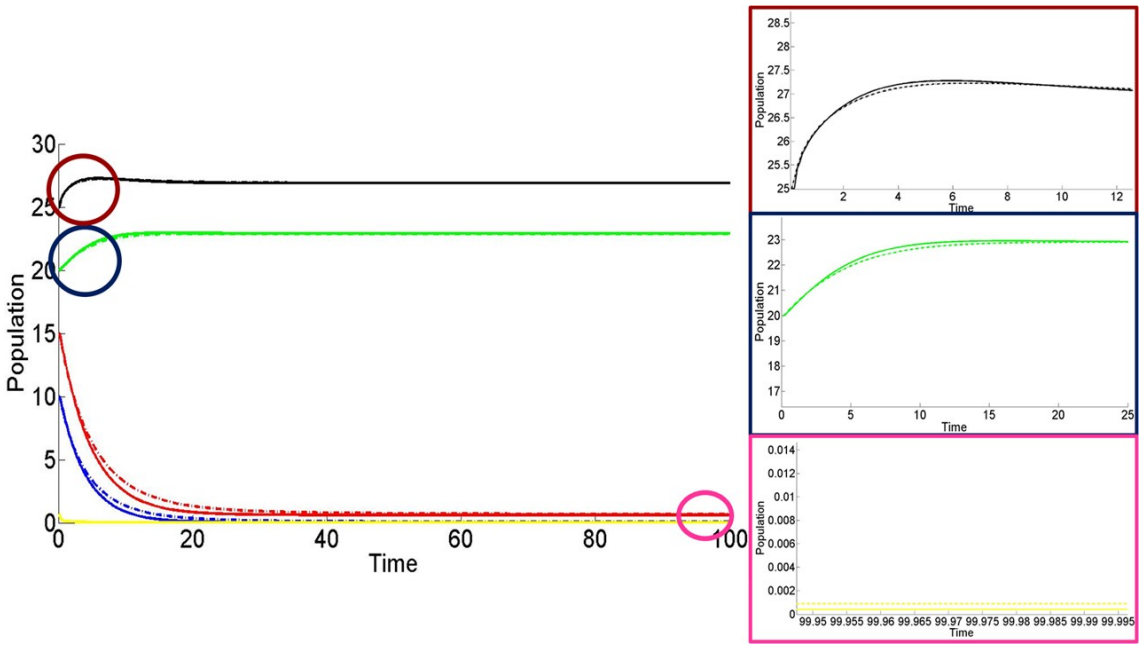

Figure 10: Evolution of all compartments; Black-Susceptible, Green-Vaccinated, Red-Exposed, Blue-Infected, Yellow-Recovered

narrow gap between upper and lower fuzzy bounds indicates that the model is stable under the assumed parameters.

Recovered Population: As illustrated in Figure 9, the recovered population rises initially and then steadily declines. This behavior is attributed to temporary immunity waning over time, where recovered individuals may either become susceptible again or exit the system. The close alignment between fuzzy solution bounds indicates that, under the given α-cut, uncertainty has a minimal effect on this compartment's long-term behavior.

Figure 10 shows the evolution of all model compartments over time. The susceptible and vaccinated populations tend toward constant values, indicating that the system has reached a disease-free equilibrium. The vaccinated class stabilizes around 23, while the susceptible class reaches approximately 27. The exposed, infected, and recovered compartments all decay toward zero, with a rapid decline in the early phase. The zoomed panels on the right side confirm the stability and convergence of these values in smaller time intervals and finer resolution. This validates the numerical consistency of the fuzzy fractal–fractional model.

6.1. Implications and Observations

The simulation results of the proposed model reveal that the infected and exposed populations rapidly decline to near-zero levels, while the susceptible and vaccinated compartments stabilize at constant values. This suggests that disease elimination may be

achievable if vaccination coverage and natural recovery rates are sustained over time. The dynamics of the recovered class, which peaks early and declines thereafter, align with the presence of temporary immunity and potential reinfection risks. The relatively narrow gap between fuzzy bounds across compartments indicates that the model remains stable even in the presence of moderate uncertainty in parameter values. These findings suggest that incorporating both memory effects and fuzzy uncertainty provides a more adaptable framework for exploring disease control strategies. While these outcomes are based on assumed inputs, they offer a foundational understanding of system behavior and indicate that, when calibrated with real epidemiological data, the model could serve as a practical tool for predicting and managing pneumonia transmission in uncertain environments. The key findings of this study are

- Disease Elimination Observed: The exposed and infected populations declined rapidly toward zero, indicating that pneumonia transmission can potentially be eliminated under sustained vaccination and recovery conditions.
- Recovered Class Decline: The recovered population initially increased and then decreased, suggesting a temporary immunity cycle and possible return to susceptibility.
- Fuzzy Stability Maintained: Despite uncertain parameters, the narrow spread between fuzzy solution bounds indicates that the system remained stable and reliable.
- Data-Driven Potential: Though the model was run under assumed conditions, it provides a solid framework that can be recalibrated using real epidemiological data for practical forecasting and control planning.

7. Comparitive Analysis

In this section, a comparison is made with the reference model 4 that uses a fractional-order SVEIR framework[44]. Both models aim to describe pneumonia transmission under vaccination and recovery influences. The comparison focuses on solution behavior, handling of uncertainty, memory effects, and system stability. Table 2 illustrates the detailed comparison between the fractional model [44] and the proposed model 5.

Table 2: Comparison between Fractional Model [44] and Proposed Model 5

Feature	**Reference Model**	**Proposed Model**
Model Type	Fractional SVEIR	Fuzzy Fractal–Fractional SVEIR
Memory Effects	Present	Enhanced via fractal structure
Fractal Dimension	Not included	Included
Fuzziness in Parameters	Not addressed	Incorporated using fuzzy numbers
Vaccinated Population Trend	Steady rise	Steady rise with uncertainty bounds
Infected Class Behavior	Decline over time	Faster convergence to zero
Recovered Class	Approaches steady state	Peaks then declines
Exposed Class	Gradual decline	Sharper drop with fuzzy progression
Numerical Method	Adams-Bashforth type	Lagrange piecewise interpolation
Uncertainty Handling	Absent	Modeled explicitly using fuzziness

8. Conclusion

This study proposed a fuzzy fractal–fractional differential framework to model the transmission dynamics of pneumonia, addressing the limitations of existing models in handling uncertainty and memory effects. Unlike classical and purely fractional models, the presented approach integrates fuzzy logic and fractal–fractional calculus to accommodate parameter imprecision and irregular dynamics observed in real-world disease spread. The model was analytically validated through theorems establishing existence, uniqueness, and Ulam–Hyers stability. Simulations using the Lagrange piecewise interpolation method showed that the infected and exposed populations decreased rapidly, converging toward zero within the first 20–30 time units. The susceptible and vaccinated populations stabilized around 27 and 23, respectively, reflecting a transition toward a disease-free equilibrium. These results demonstrate that the combination of vaccination and natural recovery, even under uncertain conditions, is sufficient to suppress disease transmission.

Compared to previous studies such as the classical fractional SVEIR model in [32], the proposed model achieved improved convergence and more realistic representation of fuzzy uncertainty in key parameters like contact and infection rates. The exposed class exhibited a sharper decline due to the inclusion of fuzziness, and the infected class showed faster stabilization, confirming the model's enhanced responsiveness. Furthermore, the recovered class initially increased and then declined, capturing temporary immunity effects absent in prior models.

The significance of this work lies in its contribution to uncertainty-aware epidemiological modeling. While many earlier models either neglected fuzziness or handled memory effects separately, this framework unifies both under a single structure. It offers a versatile tool for analyzing disease dynamics in settings where parameter values are not precisely known or are subject to environmental fluctuations.

Limitation of the current work lies in the use of theoretical assumptions without val-

idation against real clinical data. The adopted numerical method provides approximate results, which may need enhancement for handling highly stiff or complex biological systems.

Future Work

While the proposed fuzzy fractal–fractional model has shown promising results in modeling pneumonia dynamics, several avenues for future research remain open. One potential improvement is to calibrate the model using real clinical or epidemiological data, which would enhance its applicability in public health planning. The proposed modeling framework can also be extended to study other complex diseases such as tuberculosis, COVID-19, or multi-strain influenza, where uncertainty and memory effects are critical. Furthermore, integrating the current approach with deep learning techniques could facilitate real-time forecasting and decision-making in healthcare settings. For instance, hybrid models combining neural networks and fuzzy-fractal operators could better capture nonlinearity and learn from noisy datasets. Further theoretical advancements can be made by exploring optimal control strategies, sensitivity analysis, and multi-objective optimization under fuzzy fractal–fractional dynamics.

Conflict of interest

The authors declare that they have no conflicts of interest.

Acknowledgements

The article has been written with the financial support of Alagappa University Research Fund sanctioned vide Letter No.Ph.D./R20163154/AURF Fellowship/2024.
The authors thank the editor and the reviewers for their valuable comments, which have improved the quality of the work.

References

[1] E. Azoulay, L. Russell, A. Van De Louw, V. Metaxa, P. Bauer, P. Povoa, J. G. Montero, I. M. Loeches, S. Mehta, K. Puxty, P. Schellongowski, J. Rello, D. Mokart, V. Lemiale, and A. Mirouse. Diagnosis of severe respiratory infections in immunocompromised patients. *Intensive Care Medicine*, 46(2):298–314, 2020.

[2] L. Dunn. Pneumonia: classification, diagnosis and nursing management. *Nursing Standard*, 19(42):50–54, 2005.

[3] S. Sazawal and R. Black. Meta-analysis of intervention trials on case-management of pneumonia in community settings. *The Lancet*, 340(8818):528–533, 1992.

[4] A. G. Falade and A. I. Ayede. Epidemiology, aetiology and management of childhood acute community-acquired pneumonia in developing countries–a review. *African Journal of Medicine and Medical Sciences*, 40(4):293–308, 2017.

[5] M. R. Jacobs. Streptococcus pneumoniae: Epidemiology and patterns of resistance. *The American Journal of Medicine Supplements*, 117(3):3–15, 2004.
[6] K. A. Poehling, T. R. Talbot, M. R. Griffin, A. S. Craig, C. G. Whitney, E. Zell, C. A. Lexau, A. R. Thomas, L. H. Harrison, A. L. Reingold, J. L. Hadler, M. M. Farley, B. J. Anderson, and W. Schaffner. Invasive pneumococcal disease among infants before and after introduction of pneumococcal conjugate vaccine. *JAMA*, 295(14):1668, 2006.
[7] I. Rudan, C. Boschi-Pinto, Z. Biloglav, K. Mulholland, and H. Campbell. Epidemiology and etiology of childhood pneumonia. *Bulletin of the World Health Organization*, 86(5):408–416, 2008.
[8] V. Singh and S. Aneja. Pneumonia – management in the developing world. *Paediatric Respiratory Reviews*, 12(1):52–59, 2010.
[9] T. Leino, K. Auranen, J. Jokinen, M. Leinonen, P. Tervonen, and A. K. Takala. Pneumococcal carriage in children during their first two years: important role of family exposure. *The Pediatric Infectious Disease Journal*, 20(11):1022–1027, 2001.
[10] World Health Organization (WHO). Pneumonia, 2016. Accessed July 2018.
[11] K. Mulholland. Childhood pneumonia mortality—a permanent global emergency. *The Lancet*, 370(9583):285–289, 2007.
[12] World Health Organization (WHO). Pneumonia in children, 2022.
[13] T. Wardlaw, P. Salama, E. W. Johansson, and E. Mason. Pneumonia: the leading killer of children. *The Lancet*, 368(9541):1048–1050, 2006.
[14] S. Moberley, J. Holden, D. P. Tatham, and R. M. Andrews. Vaccines for preventing pneumococcal infection in adults. *Cochrane Library*, 2013.
[15] D. Aldila, N. Awdinda, N. Fatmawati, F. F. Herdicho, M. Z. Ndii, and C. W. Chukwu. Optimal control of pneumonia transmission model with seasonal factor: Learning from jakarta incidence data. *Heliyon*, 9(7):e18096, 2023.
[16] K. E. Lamb, D. Greenhalgh, and C. Robertson. A simple mathematical model for genetic effects in pneumococcal carriage and transmission. *Journal of Computational and Applied Mathematics*, 235(7):1812–1818, 2010.
[17] A. Melegaro, N. J. Gay, and G. F. Medley. Estimating the transmission parameters of pneumococcal carriage in households. *Epidemiology and Infection*, 132(3):433–441, 2004.
[18] O. J. Otieno, M. Joseph, and O. Paul. Mathematical model for pneumonia dynamics with carriers. *International Journal of Mathematical Analysis*, 7:2457–2473, 2013.
[19] A. Atangana. Fractal-fractional differentiation and integration: Connecting fractal calculus and fractional calculus to predict complex system. *Chaos Solitons & Fractals*, 102:396–406, 2017.
[20] A. Atangana and S. Qureshi. Modeling attractors of chaotic dynamical systems with fractal–fractional operators. *Chaos Solitons & Fractals*, 123:320–337, 2019.
[21] K. T. Kubra, S. Gulshan, and R. Ali. An atangana–baleanu derivative-based fractal-fractional order model for the monkey pox virus: A case study of usa. *Partial Differential Equations in Applied Mathematics*, 9:100623, 2024.
[22] S. Qureshi and A. Atangana. Fractal-fractional differentiation for the modeling and

mathematical analysis of nonlinear diarrhea transmission dynamics under the use of real data. *Chaos, Solitons & Fractals*, 136:109812, 2020.

[23] K. T. Kubra, R. Ali, R. T. Alqahtani, S. Gulshan, and Z. Iqbal. Author correction: Analysis and comparative study of a deterministic mathematical model of sars-cov-2 with fractal-fractional operators: a case study. *Scientific Reports*, 14(1), 2024.

[24] K. S. Nisar, S. Ahmad, A. Ullah, K. Shah, H. Alrabaiah, and M. Arfan. Mathematical analysis of sird model of covid-19 with caputo fractional derivative based on real data. *Results in Physics*, 21:103772, 2020.

[25] H. K. Singh and D. N. Pandey. Analysis of the chickenpox disease evolution in an mseir model using fractal-fractional differential operator. *Differential Equations and Dynamical Systems*, 2024.

[26] A. Kandel and W. Byatt. Fuzzy sets, fuzzy algebra, and fuzzy statistics. *Proceedings of the IEEE*, 66(12):1619–1639, 1978.

[27] B. Bede and L. Stefanini. Generalized differentiability of fuzzy-valued functions. *Fuzzy Sets and Systems*, 230:119–141, 2012.

[28] F. Babakordi and T. Allahviranloo. Application of fuzzy abc fractional differential equations in infectious diseases. *Computational Methods for Differential Equations*, 12(1):1–15, 2024.

[29] R. Khaliq, P. Iqbal, S. Bhat, R. Singh, S. Jain, and P. Agarwal. Generalized hukuhara derivative approach for gompertz tumor growth with allee effect under fuzzy environment. *Journal of Fuzzy Extension and Applications*, 4(4):246–256, 2023.

[30] F. Babakordi. An efficient method for solving the fuzzy ah1n1/09 influenza model using the fuzzy atangana-baleanu-caputo fractional derivative. *Fuzzy Optimization and Modelling*, 4(2):27–38, 2023.

[31] S. Subramanian, A. Kumaran, S. Ravichandran, P. Venugopal, S. Dhahri, and K. Ramasamy. Fuzzy fractional caputo derivative of susceptible-infectious-removed epidemic model for childhood diseases. *Mathematics*, 12(3):466, 2024.

[32] P. Kakati, S. G. Quek, G. Selvachandran, T. Senapati, and G. Chen. Analysis and application of rectified complex t-spherical fuzzy dombi-choquet integral operators for diabetic retinopathy detection through fundus images. *Expert Systems With Applications*, 243:122724, 2023.

[33] M. S. A. Khan, S. U. Jan, R. Jan, T. Senapati, and S. Moslem. Complex interval-valued intuitionistic fuzzy decision support system with application to covid-19 healthcare facilities. *Complex & Intelligent Systems*, 9(6):7103–7132, 2023.

[34] S. Ghorbani and D. Pamucar. Remote sensing-based evaluation of lake area dynamics: A quantitative assessment for environmental management in turkey. *Spectrum of Operational Research*, 3(1):352–358, 2025.

[35] V. Shahin, M. Alimohammadlou, and D. Pamucar. An interval-valued circular intuitionistic fuzzy marcos method for renewable energy source selection. *Spectrum of Decision Making and Applications*, 3(1):243–268, 2025.

[36] P. Mahalakshmi, J. Vimala, K. Jeevitha, and S. N. Sri. Advancing cybersecurity strategies for multinational corporations: Novel distance measures in q-rung orthopair multi-fuzzy systems. *Journal of Operational and Strategic Analytics*, 2(1):49–55, 2024.

[37] A. Surya, J. Vimala, N. Kausar, Ž. Stević, and M. A. Shah. Entropy for q-rung linear diophantine fuzzy hypersoft set with its application in madm. *Scientific Reports*, 14(1), 2024.

[38] M. Kizito and J. Tumwiine. A mathematical model of treatment and vaccination interventions of pneumococcal pneumonia infection dynamics. *Journal of Applied Mathematics*, pages 1–16, 2018.

[39] C. Ngari, G. Pokhariyal, and J. Koske. Analytical model for childhood pneumonia, a case study of kenya. *British Journal of Mathematics & Computer Science*, 12(2):1–28, 2015.

[40] D. Greenhalgh, K. E. Lamb, and C. Robertson. A mathematical model for the spread of streptococcus pneumoniae with transmission dependent on serotype. *Journal of Biological Dynamics*, 6(sup1):72–87, 2011.

[41] E. J. Ndelwa, M. Kgosimore, E. S. Massawe, and L. Namkinga. Mathematical modelling and analysis of treatment and screening of pneumonia. *Mathematical Theory and Modeling*, 5(10), 2015.

[42] G. T. Tilahun, O. D. Makinde, and D. Malonza. Modelling and optimal control of pneumonia disease with cost-effective strategies. *Journal of Biological Dynamics*, 11(sup2):400–426, 2017.

[43] O. C. Zephaniah, U. R. Nwaugonma, I. S. Chioma, and O. Adrew. A mathematical model and analysis of an sveir model for streptococcus pneumonia with saturated incidence force of infection. *Mathematical Modelling and Applications*, 5(1):16, 2020.

[44] N. Shyamsunder and S. Purohit. A novel study of the impact of vaccination on pneumonia via fractional approach. *Partial Differential Equations in Applied Mathematics*, 10:100698, 2024.

[45] T. Allahviranloo. Fuzzy fractional differential operators and equations. *Studies in Fuzziness and Soft Computing*, 2020.

[46] A. Granas and J. Dugundji. Fixed point theory. *Springer*, 2003.